Corrosion behavior of pure titanium anodes in saline medium and their performance for humic acid removal by electrocoagulation

Abdellatif El-Ghenymy[a,*], Mohammed Alshayab[b], Ahmed Khodary[c], Ignasi Sirés[d,**], Ahmed Abdel-Wahab[a]

[a] *Chemical Engineering Program, Texas A&M University at Qatar, P.O. Box 23874, Doha, Qatar*

[b] *Research Expert and Consultant, Civil and Environmental Engineering, Qatar, Doha*

[c] *Team Lead and Lab Operations at Shell, Qatar, Doha*

[d] *Laboratori d'Electroquímica dels Materials i del Medi Ambient, Departament de Química Física, Facultat de Química, Universitat de Barcelona, Martí i Franquès 1-11, 08028 Barcelona, Spain*

*Corresponding author: *E-mail address*: a.el_ghenymy@qatar.tamu.edu (A. El-Ghenymy)

**Corresponding author: *E-mail address*: i.sires@ub.edu (I. Sirés)

Abstract

The corrosion behavior of Ti electrodes and the dependence of their anodic dissolution with the experimental conditions, namely pH, current density (*j*) and supporting electrolyte nature, have been investigated. Potentiodynamic polarization and electrochemical impedance spectroscopy (EIS) tests have been performed. It has been found that pH has a relevant effect on the electrochemical dissolution of Ti. In chloride medium, metal dissolution was partially caused by pitting corrosion and the corrosion potential was shifted to more cathodic values. Conversely, in phosphate medium, corrosion was inhibited by the formation of a compact passive layer of titanium hydroxide/phosphate. Further, the mechanisms of sacrificial Ti anode dissolution during the electrocoagulation process are discussed. The influence of the supporting electrolyte, pH and *j* on the effectiveness of the electrocoagulation process for humic acid (HA) removal was assessed. Under optimized conditions, total decolorization was achieved in 60 min, eventually attaining 94% total organic carbon (TOC) removal.

Keywords: Corrosion; Electrocoagulation; Humic acid; Impedance; Titanium anode; Water treatment

1. Introduction

The formation of passive films on the surface of sacrificial anodes during the treatment of high salinity water by electrocoagulation (EC) is a real challenge since it greatly undermines the process performance (Guzmán et al., 2016; Mansouri et al., 2011a; Thiam et al., 2014; Tirado et al., 2018). Such films limit the corrosion rate, reducing the efficiency of the charge transfer at the anode interface. This results in a larger energy consumption, which hampers the viability of water treatment by EC (Mansouri et al., 2011a).

The corrosion process may involve the formation and growth of a passive oxide layer on the anode surface, which can be followed by its subsequent destruction via pitting (Amin et al., 2009; Burstein and Organ, 2005; McCafferty, 2003; McCafferty, 2010; Ren and Zuo, 2004). The presence of some dissolved anions may determine the extent and mechanism of pitting corrosion. Previous work on iron and aluminum anodes revealed the breakdown of their passive films by pitting (McCafferty, 2003; Ren and Zuo, 2004; Soltis et al., 2011).

The effect of the supporting electrolyte like sodium chloride, sulfate or phosphate on the performance of EC with Ti anode is not fully understood yet. Small and aggressive ions such as chloride can penetrate through the passive oxide film, leading to a high dissolution rate of the anode (Escrivà-Cerdán et al., 2013). Recently, growing interest has been shown regarding the optimization of experimental parameters such as pH, current density (j) and supporting electrolyte nature to avoid the formation of passive films on the anode surface during the EC process (Arroyo et al., 2009; Hanay and Hasar, 2011; Izquierdo et al., 2010; Pyun et al., 1999; Trompette and Vergnes, 2009; Zaid et al., 2008).

Among the electrochemical technologies developed as greener candidates for water and wastewater treatment, EC stands out as a technology with multiple advantages such as easy

handling, low cost and high efficiency (Rosales et al., 2018). EC is based on the dissolution of a sacrificial anode, with the simultaneous cathodic generation of hydroxide ions (OH^-) and hydrogen gas. The latter can be used as an energy vector or in the flotation and separation of the coagulated species formed during EC (Phalakornkule et al., 2010). As compared to chemical coagulation, EC allows a lower sludge production and the formation of relatively larger flocs that also contain less bound water, facilitating the subsequent filtration (Deghles and Kurt, 2016). The electrode material is one of the most relevant aspects in EC, being iron and aluminum the most widely employed due to their availability and low cost (Chen et al., 2000). The great performance of EC to decontaminate wastewater has been demonstrated in many industrial sectors, as for example olive oil production (Flores et al., 2018; Tezcan Ün et al., 2006), public water treatment facilities (Anfruns-Estrada et al., 2017), electroplating (Adhoum et al., 2004), tanneries (Apaydin et al., 2009; Espinoza-Quiñones et al., 2009; Feng et al., 2007; Murugananthan et al., 2004), copper reduction (Hatfield and Pierce, 1998) and dyeing (Küçük, 2006). One of the major challenges is the appropriate sludge management. Its disposal in agricultural areas can cause adverse environmental impacts such as groundwater contamination and, as a result, more stringent requirements are being set for sludge disposal worldwide. The presence of dissolved iron may stimulate the growth of bacteria, worsening the environmental impact (Ben Sasson and Adin, 2010). Regarding aluminum, although its salts are classified as hazardous to health, aluminum sulfates are routinely used as flocculants in sewage treatment (Cheng and Chi, 2002). Titanium salts have already been investigated as flocculants in wastewater treatment, with the recycling of the formed sludge as TiO_2 (Shon et al., 2007). On the other hand, such Ti-based flocculants exhibit a large floc, with higher affinity during the growth phase than the flocs produced by polyaluminum chloride (Zhao et al., 2011). Several studies as well as the environmental health guidelines by the World Health Organization (WHO)

reported that the amount of dissolved titanium upon flocculation agrees with the regulations for potable water and, furthermore, toxicological studies have demonstrated that Ti salts in water have not a negative health impact (Shon et al., 2007, Zhao et al., 2011). In summary, Ti-based compounds could potentially be used to replace Al- and Fe-based coagulants.

As far as we are concerned, Ti-based electrodes have not been employed in EC for water treatment yet, excluding some rare study (Kamaraj et al. 2014). In the present work, Ti has been investigated as an alternative sacrificial material to replace Al and Fe anodes for the treatment of organic compounds in water. In particular, recent studies have reported that humic acids (HA) comprise 50–90% of natural organic matter contained in water, causing a brownish or yellowish appearance. Due to their phenolate and carboxylate groups, these substances can easily react with ions and other contaminants to form complexes (Xu et al., 2011). Therefore, this article investigates the influence of the electrolyte nature, j and pH on Ti corrosion, evaluated via electrochemical impedance spectroscopy (EIS) and potentiodynamic polarization tests. In addition, the conditions to operate an EC cell equipped with Ti electrodes have been optimized for HA removal.

2. Experimental

2.1. Reagents

HA was purchased from Sigma-Aldrich. Anhydrous sodium sulfate (reagent grade, EMD, 99.0%), sodium chloride (reagent grade, Sigma-Aldrich, 99.9%), and disodium hydrogen phosphate (reagent grade, Fisher Scientific, 99.0%) were employed as supporting electrolytes. Hydrochloric acid (Sigma-Aldrich, 37%) and sodium hydroxide (VWR, 37%), were used to regulate the solution pH. The solutions used in this work were prepared with ultrapure water

produced by a Q-POD® Element water purification unit from MilliporeSigma, with resistivity > 18 MΩ cm at 25 ºC.

2.2. Experimental set-up for EC trials

All EC tests were performed under galvanostatic conditions, using an electrochemical tank reactor containing two Ti electrodes (anode and cathode) placed in parallel and separated 1.5 cm. Ti plates of 2 mm thickness (Sigma-Aldrich, 99.7%) and 10 cm^2 of active surface area were used. Before each electrolysis, the electrodes were polished using sandpaper, further being rinsed with methanol in an ultrasound bath for 15 min to remove all the impurities. Finally, the electrodes were rinsed with ultrapure water and dried at 80 ºC. Constant current from 0 to 4 A was supplied employing a DC power source (model EX354RD DUAL). The cell voltage during the electrolyses was measured using the same equipment (Fig. SM-1). Solutions of 100 mL of HA were electrocoagulated under constant stirring at 300 rpm.

Aliquots were collected during the electrolyses at different times to analyze the total organic carbon (TOC), color removal, and dissolved Ti concentration. During the evaluation of the effect of supporting electrolyte, pH and *j*, the initial pH was always adjusted to the desired value with 0.1 M NaOH or 0.1 M HCl solutions.

2.3. Analytical procedures and equipment

The pH value was measured using a SympHony thermos pH-meter. Prior to analysis, the collected samples were filtered with 0.45 μm PTFE filters supplied by VWR. Decolorization of HA solutions was monitored from their absorbance decay at the maximum wavelength (λ_{max}), which was analyzed between 200 and 800 nm at 25 ºC using a Lambda 750 UV/Vis/NIR spectrophotometer (Thiam et al., 2015a, 2015b):

$$\% \text{ Color removal} = \frac{A_0 - A_t}{A_0} \times 100 \quad (1)$$

where A_0 and A_t are the absorbance at initial time and time t at the maximum wavelength (λ_{max} = 254 nm), respectively.

The removal of HA from synthetic solutions was monitored by measuring the TOC decay, using a Shimadzu TOC-L Series analyzer equipped with an autosampler that injected samples of 50 µL. The reproducibility of the measurements was approximately ±1%. The dissolved titanium content was measured by inductively coupled plasma with optical detection (ICP-OES), using a Thermo Scientific iCAP 6000 Series device equipped with an autosampler (ASx 260), and it was compared to the theoretical amount obtained from Faraday's law following Eq. (2) (Mansouri et al., 2011b). The latter was calculated (in g L^{-1}) assuming the anodic oxidation of Ti to Ti^{4+} according to reaction (3):

$$[\text{Ti}] = \frac{ItM_{\text{Ti}}}{4FV} \quad (2)$$

where I is the applied current (A), t is electrolysis time (s), M_{Ti} is the atomic weight of Ti (= 47.86 g mol^{-1}); F is the Faraday constant (= 96487 C mol^{-1}), V is the electrolyte volume (= 0.1 L) and 4 is the number of electrons transferred per Ti atom.

$$\text{Ti} \rightarrow \text{Ti}^{4+} + 4e^- \quad (3)$$

Potentiodynamic polarization and EIS analysis were carried out using a Gamry potentiostat-galvanostat 3000 to evaluate the corrosion behaviour of Ti. The data acquisition was made with Gamry Framework and Gamry Echem Analyst software. A three-electrode electrochemical cell was used to record the potentiodynamic polarization curves of a pure Ti plate as working electrode (1 cm^2). For this purpose, a saturated calomel electrode (SCE) and platinum wire were used as the reference and counter electrodes, respectively. The scan rate was fixed at 5 mVs^{-1}, scanning toward

more positive potentials within the range from -1.5 V to +1.5 V vs SCE. All trials were carried out at open circuit potential after 1800 s of immersion of the electrode in the supporting electrolyte. The amplitude of the AC signal was 10 mV to analyse the electrode response within the range from ~0.02 Hz up to 100 kHz.

3. Results and discussion

3.1. Potentiodynamic polarization and electrochemical impedance spectroscopy

3.1.1. Effect of pH

The potentiodynamic polarization technique was employed for corrosion testing, aiming to acquire relevant information to better understand the electrodissolution of titanium anode. Several experiments, including potentiodynamic polarization and open circuit potential measurements, were carried out. Fig. 1a shows the effect of solution pH, within the range 2-11, on the potentiodynamic polarization curves recorded in 0.5 M NaCl aerated aqueous solutions using pure titanium as working electrode. A shift of the corrosion potential (E_{corr}) could be observed when pH became more alkaline or more acidic than 7. The trials conducted at pH 2, 5, and 7 showed the lowest E_{corr}, and no pitting corrosion was observed at these pH values. Hydrogen generation was the main reaction accounting for the profile of the cathodic branch (Heljo et al., 2014):

$$2H^+ + 2e^- \rightarrow H_2\uparrow \quad (4)$$

A different behavior was observed for the anodic branch, showing a trend that can be typically associated to metal passivation. The formation of a passive oxide film affected to the corrosion propagation. The main reactions accounting for the profile of the anodic branch are (Heljo et al., 2014):

$$Ti \rightarrow Ti^{3+} + 3e^{-} \quad (5)$$

$$2Ti^{3+} + 3H_2O \rightarrow Ti_2O_3 + 6H^{+} \quad (6)$$

$$Ti^{3+} \rightarrow Ti^{4+} + e^{-} \quad (7)$$

$$Ti^{4+} + 2H_2O \rightarrow TiO_2 + 4H^{+} \quad (8)$$

Ti^{3+}/Ti^{4+} ions generated during the titanium electrodissolution gave rise to a stationary passive oxide film composed of Ti_2O_3 and TiO_2. The TiO_2/Ti_2O_3 film protects the electrode surface and inhibits further corrosion. However, chloride ions are known to be aggressive, moving through the passive oxide film in parallel with oxide ions and speeding up the anodic dissolution (Escrivà-Cerdán et al., 2013; Liu et al., 2001), as follows:

$$Ti_xO_y + 2Cl^{-} \rightarrow Ti_xO_yCl_2 + 2e^{-} \quad (9)$$

The E_{corr} was shifted to more cathodic values when pH was increased from acidic or neutral values to pH 8-11, which evidences the larger dissolution of the passive film upon the action of OH^{-} ions. This attack caused the conversion of the compact film into a thinner one, so-called alkaline chemical dissolution.

The EIS spectra of Fig. 1b reveal that at high frequency, the diameter of the semi-circle was reduced at pH 8-11, owing to the less effective passivation of the titanium plate, which is in agreement with the progressively thinner oxide film resulting from the attack of OH^{-} ions.

3.1.2. Effect of supporting electrolytes concentration

As previously mentioned, the chloride ions are consider as aggressive and, due to their small size, they are enabled to penetrate easily through the passive layer under the effect of an electric field, eventually causing pitting corrosion (Loto, 2013). The presence of chloride ions stimulates the hydrolysis of the corrosion products, thus inhibiting the effective passivation. Fig. 2a illustrates

185 the cathodic and anodic potentiodynamic polarization curves obtained for a Ti electrode in aerated
186 ultrapure water without supporting electrolyte. A typical Tafel behavior is evidenced for both,
187 cathodic and anodic curves. In contrast, in the presence of chloride, the anodic branches differed
188 significantly to the previous one (Fig. 2a). The anodic curves did not agree with a Tafel behavior
189 within the entire potential range, which is related to the corrosion of Ti anode and the gradual
190 formation ad growth of the oxide layer. The current was maintained occasionally constant within
191 the passivation region. The potentiodynamic polarization curves in chloride medium did not
192 display prototypical passivation, where an initially active region is immediately followed by a
193 passive one due to the growth of an oxide film. Here, this was followed by its breakdown at around
194 1.0 V. This behavior confirms that the film produced on Ti anode was not defensive and integral.
195 The corrosion resistance of each material is largely dependent on various ingredients including the
196 structure, microstructure, and environment (Geetha et al., 2004). For this kind of corrosion, the
197 environment is the most significant agent.

198 Four potential intervals can be distinguished in the potentiodynamic curves obtained in Fig.
199 2a: (i) Cathodic potentials at which the oxygen reduction is prevalent; (ii) E_{corr} value; (iii)
200 passivation regions in the anodic curve, where current is unaffected by the applied potential; and
201 (iv) highly positive potential values that cause the breakdown of the passive film, with the
202 consequent current increase. It can be noted that the anodic current at any applied potential rose
203 when the Cl^- concentration was increased from 0.5 to 1 M (Fig. 2a), as expected from the greater
204 pitting corrosion.

205 As can be observed in Fig. 2b, an increase of the NaCl concentration led to a decrease of the
206 semi-circle diameter in the Nyquist plot. This behavior is related to the double layer created by the
207 interaction between the porous external layer of the surface film and dissolved chloride ions. The

Bode plot depicted in Fig. 2c can be divided into two regions, i.e., at low frequency (< 100 Hz) and at high frequency (> 100 Hz). At high frequency (10^2 up to 10^5 Hz), the curves presented a planar form with a slope around zero, which can be related to the electrolyte resistance (Robin et al., 2008; Munirathinam et al., 2016); at low frequency, the curves were linear with a slope near 1, which can be explained by the capacitive effect of the passive layer (Robin et al., 2008; Munirathinam et al., 2016). The Bode phase plots can be also divided into two regions: (i) at high frequency, the phase angle is close to zero due to electrolyte resistance response, whereas (ii) at low and medium frequency, the phase angle drops to low values because of the passive film response. Hence, the EIS results corroborate the potentiodynamic analyses.

3.1.3. Effect of supporting electrolyte nature

Fig. 3a shows the cathodic and anodic branches of polarization curves obtained for Ti in different supporting electrolytes. It is evident that the nature of the electrolyte affected the E_{corr} and corrosion current (I_{corr}) values. As summarized in Table 1, E_{corr} was shifted to more negative values in the presence of chloride and sulfate ions, which means that these ions promote the Ti corrosion. In contrast, the presence of Na_2HPO_4 shifted the E_{corr} toward more positive values, which suggests an inhibitory effect. The worst conditions regarding the stability of Ti anode were found in NaCl + Na_2SO_4, yielding the most negative E_{corr} (= -405 mV) and the highest I_{corr} (= 0.152 µA cm^{-2}) due to the combined effect of aggressive chloride ion and enhanced solution conductivity. Fig. 3a shows that the current of the anodic branch increased when the medium was changed from 0.5 M Na_2HPO_4 to 0.5 M (NaCl + Na_2SO_4 + Na_2HPO_4), thus confirming the relevance of chloride ion that accounts for a higher corrosion rate (McCafferty, 2003).

Fig. 3b illustrates the Nyquist plot for Ti anode in the previous media. Within the high frequency region, the plots show a small semi-circle with a diameter decrease from 0.5 M

231 Na_2HPO_4 to 0.5 M (NaCl + Na_2SO_4 + Na_2HPO_4), corroborating the loss of passive layer resistance
232 and the consequent enhancement of Ti dissolution. At low frequency, the Nyquist plots show a
233 diffusional behavior with a tendency of 45° towards the real impedance. The diffusional feature is
234 related to the electrodissolution of Ti anode and the diffusion of their generated species toward the
235 solution.

236 As depicted in Fig. 3c, the Bode plot can be divided into two regions, in agreement with that
237 found in Fig. 2c. A planar trend (slope ~0) appeared at high frequency, whereas a linear tendency
238 (slope ~1) was observed at low frequency. The magnitude of the impedance within the latter region
239 increased slightly due to passive layer resistance. The Bode phase plots can be explained as above.

240 *3.2. HA removal by electrocoagulation*

241 *3.2.1. Effect of pH*

242 In general, the solution pH plays a key role in the anode dissolution as well as in the whole
243 EC process. Several trials were conducted to clarify the pH effect on the EC treatment of 30 mg
244 L^{-1} HA (i.e., 16.8 mg L^{-1} TOC) solutions with 0.5 mol NaCl within the pH range 2-11 using Ti
245 electrodes at 5 mA cm^{-2}. Fig. 4a and 4b show the effect on color and TOC removal, respectively,
246 which were enhanced as the pH increased from 2 to 9 but diminished for more alkaline solutions.
247 For example, TOC removal at pH 2, 5, 7, 8, 9, 10, and 11 was 61.7%, 64.8%, 66.7%, 70.1%,
248 77.3%, 74.2% and 72.2%, respectively. The highest performance of EC was achieved at pH 9,
249 attaining ~77% and 96% of TOC and color removal, respectively. Fig. 4c shows an initial increase
250 of pH at the beginning of all the electrolyses, thereby becoming stable. This behavior is dependent
251 on the Ti hydroxide complexes generated during the EC treatment. In alkaline medium, Ti was
252 preeminently found as $Ti(OH)_3$, $Ti(OH)_4$, and $TiO_2•H_2O$, which adsorbed deprotonated HA on
253 their surface. Most Ti species produced during the anode electrodissolution precipitate as titanium

hydroxides at pH 9. Pourbaix diagrams for Ti illustrate that, at pH > 8, $Ti(OH)_4$ and $Ti(OH)_3$ are the prevalent species (Chen et al., 2005). In contrast, under acidic conditions, $Ti(OH)_4$ and $Ti(OH)_3$ do not precipitate, impeding the efficient coagulation. Ti complexes formed are positively charged at acid pH and negatively charged at highly alkaline pH, being neutral at pH 6-8 (Jezequel and Chu, 2006; Kamaraj et al., 2014). The effect of pH on electrocoagulation process is in accordance with Ti dissolution revealed by polarization tests (Fig. 1a and 1b).

3.2.2. Effect of current density

It is well known that the applied current is a determinant for any electrochemical process. In EC, this parameter can define the flocs size and their development, as well as the production rate of H_2 bubbles, eventually affecting to the EC performance. Ti electrodissolution can produce a large set of Ti species, including 7 dissolved ones and 9 solids. In aqueous solution, these substances interact with hydroxide ions to form Ti complexes (Chen et al., 2005). Among them, Ti_2O_3, Ti_3O_5, $TiO_3{\bullet}H_2O$, and $Ti(OH)_2$ are easily soluble, generating ions, whereas $TiO_2{\bullet}H_2O$, $Ti(OH)_3$ and $Ti(OH)_4$ are more stable as such. Ti electrodissolution agrees with the following consecutive reactions (Chen et al., 2005; Fekry, 2009; Kamaraj et al., 2014):

$$Ti \rightarrow Ti^{2+} \rightarrow TiO^{2+} \quad (10)$$

Hydroxide ions OH^- bind quickly to TiO^{2+}, giving rise to $Ti(OH)_4$ and $TiO_2{\bullet}H_2O$ via reaction (11) and (12) (Chen et al., 2005).

$$TiO^{2+} + 6OH^- + 2e^- \rightarrow Ti(OH)_4 + H_2 + 3O^{2-} \quad (11)$$

$$TiO^{2+} + 2OH^- \rightarrow TiO_2{\bullet}H_2O \quad (12)$$

In chloride medium. TiO^{2+} can be easily hydrolyzed (Fekry, 2009; Qu et al., 2014):

$$TiO^{2+} + Cl^- + 2H_2O \rightarrow [Ti(OH)_3]Cl + H^+ \quad (13)$$

The TOC and color removal is expected to be largely dependent on the amount of the produced coagulants (Ti complexes), which in turn depends on the current density and the electrolysis time (Kamaraj et al., 2014; Vasudevan et al., 2013). In order to clarify the influence of *j*, several EC trials were made within the range 1-10 mA cm^2 using HA solutions (16.8 mg L^{-1} TOC) in 0.5 M NaCl as supporting electrolyte at optimal pH 9. Fig. 5a and 5b present the evolution of the UV/Vis spectrum during EC at the lowest and the highest *j*, respectively, whereas Fig. 5c depicts the course of the decolorization efficiency calculated from Eq. (1) at λ_{max} = 254 nm. As can be seen, overall decolorization was achieved at 5, 7.5 and 10 mA cm^{-2}, at a shorter time as *j* rose. This suggests that a higher quantity of Ti complexes was gradually formed, which resulted in a faster TOC and color removal. The oxygen and hydrogen evolution, with the corresponding bubbles speeding up the contact between HA and Ti complexes, also depend on *j*. Gas bubbles improve the suspension of the formed flocs, which was observed during the EC treatments. Yellowish to brownish precipitates fell down to the bottom of the reactor, whereas less dense aggregates became accumulated on the top of the solution. Fig. 5c also shows an incomplete decolorization at too low *j* of 1 and 2.5 mA cm^{-2}, suggesting that the electrogenerated Ti species were insufficent to flocculate and eliminate all the HA.

The TOC abatements were 36.8%, 64.0%, 77.3%, 87.5% and 93.9% at 1, 2.5, 5, 7.5 and 10 mA cm^{-2}, respectively, after a specific charge consumption of 1.5 Ah L^{-1} (Fig. 5d). These results confirm that both, TOC and the color removal were upgraded as *j* rose. Fig. 5e illustrates the influence of *j* on pH evolution during the same EC treatments. The solutions, whose initial pH was 9, always became more alkaline during the first minutes of EC treatment in a very quick manner. Subsequently, the pH started to slightly decrease, ending in 8.2, 8.4, 8.5, 8.6, and 8.8 for trials performed at 1, 2.5, 5, 7.5, and 10 mA cm^{-2}, respectively. Fig. 5f shows the trends of the

299 experimental and theoretical amount of dissolved Ti accumulated during the electrolyses in 0.5 M
300 NaCl at 7.5 mA cm^{-2}. A linear trend was verified for Ti dissolution with the specific electrical
301 charge (Ah L^{-1}), exhibiting a very good agreement between both data sets. The small difference
302 between the theoretical and experimental can be attributed to the formation of the protective layer
303 on the anode surface during EC. Several researchers have reported that, in EC with Fe or Al, the
304 experimental anode dissolution can be related to both, chemical and electrochemical dissolution.
305 Aiming to assess this hypothesis, a Ti plate of known weight was immersed into a 0.5 M NaCl
306 solution at pH 9 for 180 min, whereupon the dissolved Ti was measured. The value was as low as
307 0.06 mg L^{-1}, meaning that the generated Ti in EC can be simply related to the electrochemical
308 dissolution.

309 *3.2.3. Effect of supporting electrolyte nature*

310 Several trials have been carried out to evaluate the influence of the electrolyte nature (NaCl,
311 Na_2SO_4 and Na_2HPO_4, and their combinations) on TOC and color abatement during EC. Solutions
312 with different supporting electrolytes containing 16.8 mg L^{-1} TOC of HA were electrolyzed at pH
313 9 and 10 mA cm^{-2}. First, sodium sulfate was employed as single supporting electrolyte, but the cell
314 voltage was excessively high (35 V), which can be explained by the formation of a quite stable
315 film on the anode surface that caused its effective passivation. On the other hand, when Na_2SO_4
316 was replaced by Na_2HPO_4, the color and TOC removals (Fig. 6a and 6b) were poor. This was due
317 to a very slow anodic dissolution, as a result of the substitution of Ti-OH on the titanium anode
318 surface by insoluble phosphates. Most of the dissolved titanium species were transformed into
319 titanium phosphates as follows:

320 $$TiO(OH)_2 + HPO_4^{2-} \rightarrow TiO(HPO_4) + 2OH^- \quad (14)$$

Fig. 6c demonstrates that the pH during the EC trials was slightly influenced by the supporting electrolyte nature, rising from 9 up to 9.3 and 9.5 when 0.3 M and 0.5 M of Na_2HPO_4 was added to the 0.5 M NaCl solution, respectively. As can be observed in Fig. 6a and 6b, the efficiency of TOC and color removal in chloride medium was higher than that in phosphate or sulfate media. At 90 min, EC yielded 93.9%, 24.9%, 93.5%, and 87.4% TOC abatement in NaCl, Na_2HPO_4, (NaCl + Na_2SO_4) and (NaCl + Na_2SO_4 + Na_2HPO_4), respectively. The high performance of EC in the presence of chloride is related to the effective breakdown of the passive compact film formed upon anode dissolution, in agreement with the polarization and impedance results commented above. The aggressive chloride ions migrate inside the pit through the passive film, destabilizing it and eventually promoting the Ti dissolution and hence, the HA removal by EC.

4. Conclusions

This work has demonstrated that the corrosion of Ti is dependent on pH and electrolyte nature. In phosphate medium, the corrosion was not favored, owing to the formation of a passive film, whereas chloride ions enhanced the corrosion rate and E_{corr} was shifted to a more active value due to pitting corrosion. Electrodissolution experiments revealed that the amount of dissolved Ti was slightly lower than the theoretical one. The pH evolution during the electrodissolution of Ti anode was related to the electrolyte nature and the initial pH. The pH increased continuously in phosphate medium, whereas in chloride or sulfate media, the pH increased at the beginning and then became stable. It is also demonstrated that EC with Ti as sacrificial anode material can be a suitable process to remove HA from water. The color and TOC removals depended on the electrolyte nature, *j* and pH. Total decolorization of HA was achieved in 60 min and 94% TOC was removed at 90 min operating in 0.5 M NaCl at pH 9.0 and 10 mA cm^{-2} after consumption of 1.5 Ah L^{-1}. Therefore,

343 the Ti species formed during EC treatment have a high effectiveness for HA removal by
344 precipitation, adsorption, coagulation, and/or flotation, thus being a potential alternative to EC
345 with Fe or Al.

346 **Acknowledgements**

347 The authors are grateful to Texas A&M University in Qatar, as well as to Qatar Foundation
348 for providing financial support to perform this research.

349 **References**

350 Adhoum, N., Monser, L., Bellakhal, N., Belgaied, J.-E., 2004. Treatment of electroplating
351 wastewater containing Cu^{2+}, Zn^{2+} and Cr(VI) by electrocoagulation, J. Hazard. Mater. 112,
352 207–213.

353 Amin, M.A., Abd El-Rehim, S.S., El-Sherbini, E.F., Mahmoud, S.R., Abbas, M.N., 2009. Pitting
354 corrosion studies on Al and Al-Zn alloys in SCN^- solutions. Electrochim. Acta 54, 4288–
355 4296.

356 Anfruns-Estrada, E., Bruguera-Casamada, C., Salvadó, H., Brillas, E., Sirés, I., Araujo, R.M.,
357 2017. Inactivation of microbiota from urban wastewater by single and sequential
358 electrocoagulation and electro-Fenton treatments. Water Res. 126, 450–459.

359 Apaydin, O., Kurt, U., Gonullu, M.T., 2009. An investigation on the treatment of tannery
360 wastewater by electrocoagulation, Global Nest J. 11, 546–555.

361 Arroyo, M.G., Pérez-Herranz, V., Montañés, M.T., García-Antón, J., Guiñón, J.L., 2009. Effect of
362 pH and chloride concentration on the removal of hexavalent chromium in a batch
363 electrocoagulation reactor. J. Hazard. Mater. 169, 1127–1133.

364 Ben Sasson, M., Adin, A., 2010. Fouling mitigation by iron-based electroflocculation in
365 microfiltration: Mechanisms and energy minimization, Water Res. 44, 3973–3981.
366 Burstein, G.T., Organ, R.M., 2005. Repassivation and pitting of freshly generated aluminium
367 surfaces in acidic nitrate solution. Corr. Sci. 47, 2932–2955.
368 Chen, C.–C., Chen, J.–H., Chao, C.–G., Say, W.C., 2005. Electrochemical characteristics of
369 surface of titanium formed by electrolytic polishing and anodizing. J. Mater. Sci. 40, 4053–
370 4059.
371 Chen, B.G., Chen, X., Yue, P.L., 2000. Electrocoagulation and electroflotation of restaurant
372 wastewater, J. Environ. Eng. 126, 858-863.
373 Cheng, W.P., Chi, F.H., 2002. A study of coagulation mechanisms of polyferric sulfate reacting
374 with humic acid using a fluorescence-quenching method, Water Res. 36, 4583–4591.
375 Deghles, A., Kurt, U., 2016. Treatment of tannery wastewater by a hybrid
376 electrocoagulation/electrodialysis process. Chem. Eng. Process. 104, 43–50.
377 Escrivà-Cerdán, C., Blasco-Tamarit, E., García-García, D.M., García Antón, J., Akid, R., Walton,
378 J., 2013. Effect of temperature on passive film formation of UNS N08031 Cr–Ni alloy in
379 phosphoric acid contaminated with different aggressive anions. Electrochim. Acta 111, 552–
380 561.
381 Espinoza-Quiñones, F.R., Fornari, M.M.T., Módenes, A.N., Palácio, S.M., da Silva, F.G.,
382 Szymanski, N., Kroumov, A.D., Trigueros, D.E.G., 2009. Pollutant removal from tannery
383 effluent by electrocoagulation, Chem. Eng. J. 151, 59–65.
384 Fekry, A.M., 2009. The influence of chloride and sulphate ions on the corrosion behavior of Ti
385 and Ti-6Al-4V in oxalic acid. Electrochim. Acta 54, 3480–3489.

386 Feng, J., Sun, Y., Zheng, Z., Zhang, J., Li, S., Tian, Y., 2007. Treatment of tannery wastewater by
387 electrocoagulation, J. Environ. Sci. 19, 1409–1415.
388 Flores, N., Brillas, E., Centellas, F., Rodríguez, R.M. Cabot, P.L., Garrido, J.A., Sirés, I., 2018.
389 Treatment of olive oil mill wastewater by single electrocoagulation with different electrodes
390 and sequential electrocoagulation/electrochemical Fenton-based processes. J. Hazard. Mater.
391 347, 58–66.
392 Geetha, M., Kamachi, U.M., Gogia, A.K., Asokamani, R., Baldev, R., 2004. Influence of
393 microstructure and alloying elements on corrosion behaviour of Ti–13Nb–13Zr alloy, Corr.
394 Sci. 46, 877–892.
395 Guzmán, A., Nava, J.L., Coreño, O., Rodríguez, I., Gutiérrez, S., 2016. Arsenic and fluoride
396 removal from groundwater by electrocoagulation using a continuous filter-press reactor.
397 Chemosphere 144, 2113-2120.
398 Hanay, O., Hasar, H., 2011. Effect of anions on removing Cu^{2+}, Mn^{2+} and Zn^{2+} in
399 electrocoagulation process using aluminum electrodes. J. Hazard. Mater. 189, 572–576.
400 Hatfield, T.L., Pierce, D.T., 1998. Electrochemical remediation of metal bearing wastewaters Part
401 II: Corrosion-based inhibition of copper removal by iron (III). J. Appl. Electrochem. 28, 397–
402 403.
403 Heljo, P.S., Wolff, K., Lahtonen, K., et al., 2014. Anodic oxidation of ultra-thin Ti layers on ITO
404 substrates and their application in organic electronic memory elements, Electrochim. Acta
405 137, 91–98.
406 Izquierdo, C.J, Cañizares, P., Rodrigo, M.A., Leclerc, J.P., Valentin, G., Lapicque, F., 2010. Effect
407 of the nature of the supporting electrolyte on the treatment of soluble oils by
408 electrocoagulation. Desalination 255, 15–20.

409 Jezequel, H., Chu, K. H., 2006. Removal of arsenate from aqueous solution by adsorption onto
410 titanium dioxide nanoparticles. J. Environ. Sci. Health A 41, 1519-1528.
411 Kamaraj, R., Ganesan, P., Vasudevan, S., 2014. Use of hydrous titanium dioxide as potential
412 sorbent for the removal of manganese from water. J. Electrochem. Sci. Eng. 4, 187-201.
413 Küçük, Ö., 2006. Application of Taguchi method in the optimization of dissolution of ulexite in
414 NH_4Cl solutions, Korean J. Chem. Eng. 23, 21–27.
415 Liu, C., Leyland, A., Bi, Q., Matthews, A., 2001. Corrosion resistance of multi-layered plasma-
416 assisted physical vapour deposition TiN and CrN coatings. Surf. Coat. Technol. 141,164–173.
417 Loto, R.T., 2013. Pitting corrosion evaluation of austenitic stainless steel type 304 in acid chloride
418 media. J. Mater. Environ. Sci. 4, 448-459.
419 Mansouri, K., Elsaid, K., Bedoui, A., Bensalah, N., Abdel-Wahab, A., 2011a. Application of
420 electrochemically dissolved iron in the removal of tannic acid from water. Chem. Eng. J. 172,
421 970–976.
422 Mansouri, K., Ibrik, K., Bensalah, N., Abdel-Wahab, A., 2011b. Anodic dissolution of pure
423 aluminum during electrocoagulation process: Influence of supporting electrolyte, initial pH,
424 and current density. Ind. Eng. Chem. Res. 50, 13362–13372.
425 McCafferty, E., 2003. Sequence of steps in the pitting of aluminum by chloride ions. Corr. Sci. 45,
426 1421–1438.
427 McCafferty, E., 2010. Pit initiation on aluminum as a queuing process. J. Electrochem. Soc. 157,
428 C382–C387.
429 Munirathinam, B., Narayanan, R., Neelakantan, L., 2016. Electrochemical and semiconducting
430 properties of thin passive film formed on titanium in chloride medium at various pH
431 conditions. Thin Solid Films 598, 260–270.

Murugananthan, M., Bhaskar Raju, G., Prabhakar, S., 2004. Separation of pollutants from tannery effluents by electro flotation, Sep. Purif. Technol. 40, 69–75.

Phalakornkule, C., Sukkasem, P., Mutchimsattha, C., 2010. Hydrogen recovery from the electrocoagulation treatment of dye-containing wastewater, Int. J. Hydrogen Energy 35, 10934–10943.

Pyun, S.I., Moon, S.M., Ahn, S. H., Kim, S. S., 1999. Effects of Cl^-, NO_3^-, and SO_4^{2-} ions on anodic dissolution of pure aluminum in alkaline solution. Corr. Sci. 41, 653–667.

Qu, Q., Wang, L., Chen, Y., Li, L., He, Y., Ding, Z., 2014. Corrosion behavior of titanium in artificial saliva by lactic acid. Materials 7, 5528-5542.

Ren, J., Zuo, Y., 2004. Study of electrochemical behavior and morphology of pitting on anodized 2024 aluminum alloy. Surf. Coat. Technol. 182, 237–241.

Robin, A., Carvalho, O.A.S., Schneider, S.G., Schneider, S., 2008. Corrosion behavior of Ti-xNb-13Zr alloys in Ringer's solution. Mater. Corr. 59, 929–933.

Rosales, M., Coreño, O., Nava, J.L., 2018. Removal of hydrated silica, fluoride and arsenic from groundwater by electrocoagulation using a continuous reactor with a twelve-cell stack. Chemosphere 211, 149-155.

Shon, H.K., Vigneswaran, S., Kim, I.S., Cho, J., Kim, G.J., Kim, J.B., Kim, J.H., 2007. Preparation of titanium dioxide (TiO_2) from sludge produced by titanium tetrachloride ($TiCl_4$) flocculation of wastewater, Environ. Sci. Technol. 41, 1372–1377.

Thiam, A., Sirés, I., Brillas, E., 2015a. Treatment of a mixture of food color additives (E122, E124 and E129) in different water matrices by UVA and solar photoelectro-Fenton. Water Res. 81, 178–187.

454 Thiam, A., Sirés, I., Centellas, F., Cabot, P.L., Brillas, E., 2015b. Decolorization and
455 mineralization of Allura Red AC azo dye by solar photoelectro-Fenton: Identification of
456 intermediates. Chemosphere 136, 1–8.
457 Thiam, A., Zhou, M., Brillas, E., Sirés, I., 2014. A first pre-pilot system for the combined treatment
458 of dye pollutants by electrocoagulation/EAOPs. J. Chem. Technol. Biotechnol. 89, 1136–
459 1144.
460 Tirado, L., Gökkus, Ö., Brillas, E., Sirés, I., 2018. Treatment of cheese whey wastewater by
461 combined electrochemical processes. J. Appl. Electrochem. 48, 1307–1319.
462 Trompette, J.L., Vergnes, H., 2009. On the crucial influence of some supporting electrolytes during
463 electrocoagulation in the presence of aluminum electrodes. J. Hazard. Mater. 163, 1282–1288.
464 Tezcan Ün, Ü., Uğur, S., Koparal, A.S., Bakır Öğütveren, Ü., 2006. Electrocoagulation of olive
465 mill wastewaters, Sep. Purif. Technol. 52, 136–141.
466 Vasudevan, S., Lakshmi, J., Sozhan, G., 2013. Electrochemically assisted coagulation for the
467 removal of boron from water using zinc anode, Desalination, 310, 122–129.
468 Xu, W.Y., Gao, B.Y., Yue, Q.Y., Wang, Q.A., 2011. Effect of preformed and non-preformed
469 Al(13) species on evolution of floc size, strength and fractal nature of humic acid flocs in
470 coagulation process, Sep. Purif. Technol. 78, 83–90.
471 Zaid, B., Saidi, D., Benzaid, A., Hadji, S., 2008. Effects of pH and chloride concentration on pitting
472 corrosion of AA6061 aluminum alloy. Corr. Sci. 50, 1841–1847.
473 Zhao, Y.X., Gao, B.Y., Shon, H.K., Kim, J.H., Yue, Q.Y., 2011. Effect of shear force, solution pH
474 and breakage period on characteristics of flocs formed by titanium tetrachloride ($TiCl_4$) and
475 polyaluminum chloride (PACl) with surface water treatment. J. Hazard. Mater. 187, 495–501.
476

Figure captions

Fig. 1. Influence of pH on (a) potentiodynamic polarization curve and (b) Nyquist plot obtained for pure titanium as working electrode (1 cm^2) in aerated aqueous solutions containing 0.5 M NaCl as a supporting electrolyte. Counter electrode: Pt wire; reference electrode: SCE; scan rate: 5 mV s^{-1}.

Fig. 2. Influence of supporting electrolyte concentration on (a) potentiodynamic polarization curve, b) Nyquist plot and c) Bode plot for pure titanium as working electrode (1 cm^2) in aerated aqueous solutions at pH 9.0. Counter electrode: Pt wire; reference electrode: SCE; scan rate: 5 mV s^{-1}.

Fig. 3. Influence of supporting electrolyte nature (each at a concentration of 0.5 M) on (a) potentiodynamic polarization curve, b) Nyquist plot and c) Bode plot for pure titanium as working electrode (1 cm^2) in aerated aqueous solutions at pH 9.0. Counter electrode: Pt wire; reference electrode: SCE; scan rate: 5 mV s^{-1}.

Fig. 4. (a) Time course of color removal, along with (b) TOC removal and (c) pH evolution with specific charge during the electrocoagulation of aqueous solutions containing 16.8 mg L^{-1} TOC of humic acid (HA) in 0.5 M NaCl as supporting electrolyte at different initial pH values, using pure Ti as the anode at j = 5 mA cm^{-2}.

Fig. 5. Electrocoagulation of aqueous solutions containing 16.8 mg L^{-1} TOC of humic acid (HA) in 0.5 M NaCl as supporting electrolyte at pH 9.0, using pure Ti as the anode. (a,b) UV/Vis spectra recorded at 1 mA cm^{-2} and 10 mA cm^{-2}, respectively. Effect of current density on (c) color removal, (d) TOC removal, and (e) pH evolution. (f) Theoretical and experimental values of dissolved Ti content at j = 7.5 mA cm^{-2}.

Fig. 6. Influence of supporting electrolyte nature (each at a concentration of 0.5 M, except in plot c) on (a) color removal, (b) TOC removal and c) pH evolution during the electrocoagulation of aqueous solutions containing 16.8 mg L^{-1} TOC of humic acid (HA) at pH 9.0, using pure Ti as the anode at j = 10 mA cm^{-2}.

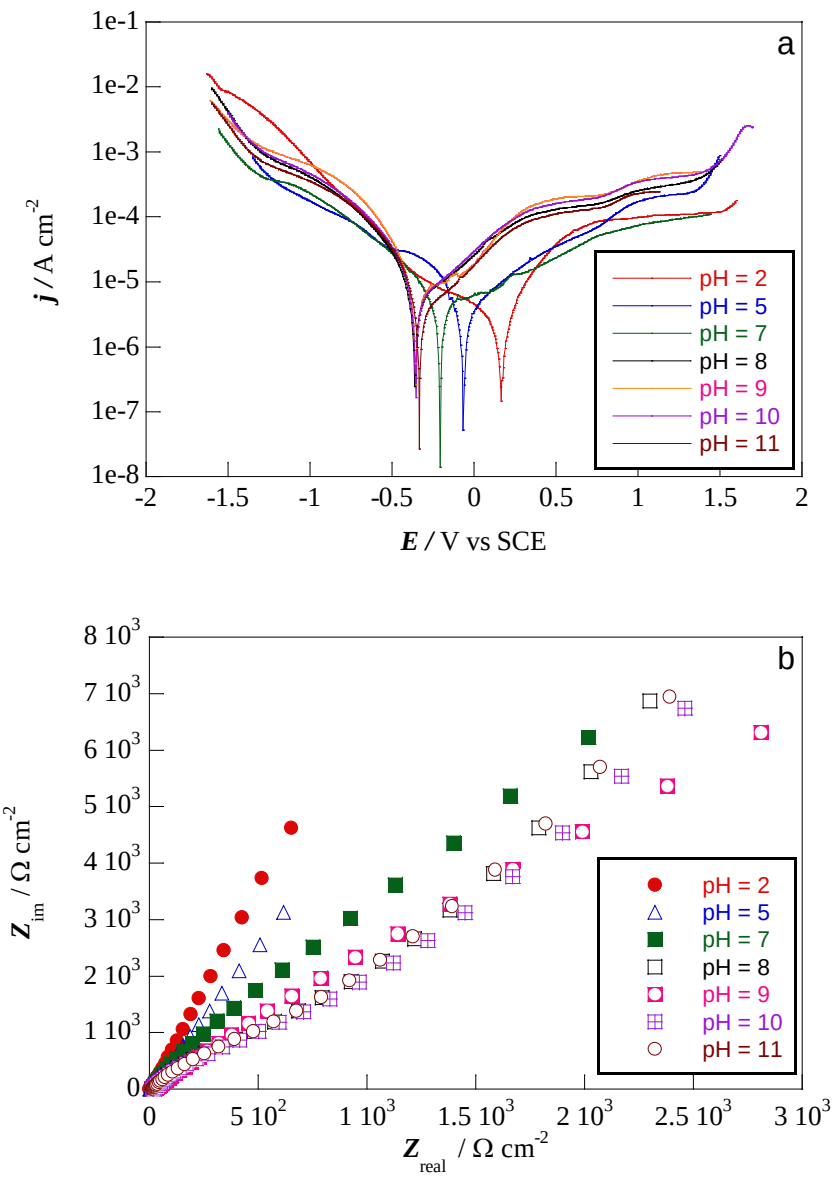
a
1e-1
1e-2
1e-3
1e-4
1e-5
1e-6
1e-7
1e-8
j / A cm-2
-2
-1.5
-1
-0.5
0
0.5
1
1.5
2
E / V vs SCE
pH = 2
pH = 5
pH = 7
pH = 8
pH = 9
pH = 10
pH = 11
b
8 10^3
7 10^3
6 10^3
5 10^3
4 10^3
3 10^3
2 10^3
1 10^3
0
Z_im / Ω cm-2
0
5 10^2
1 10^3
1.5 10^3
2 10^3
2.5 10^3
3 10^3
Z_real / Ω cm-2
pH = 2
pH = 5
pH = 7
pH = 8
pH = 9
pH = 10
pH = 11

Fig. 1

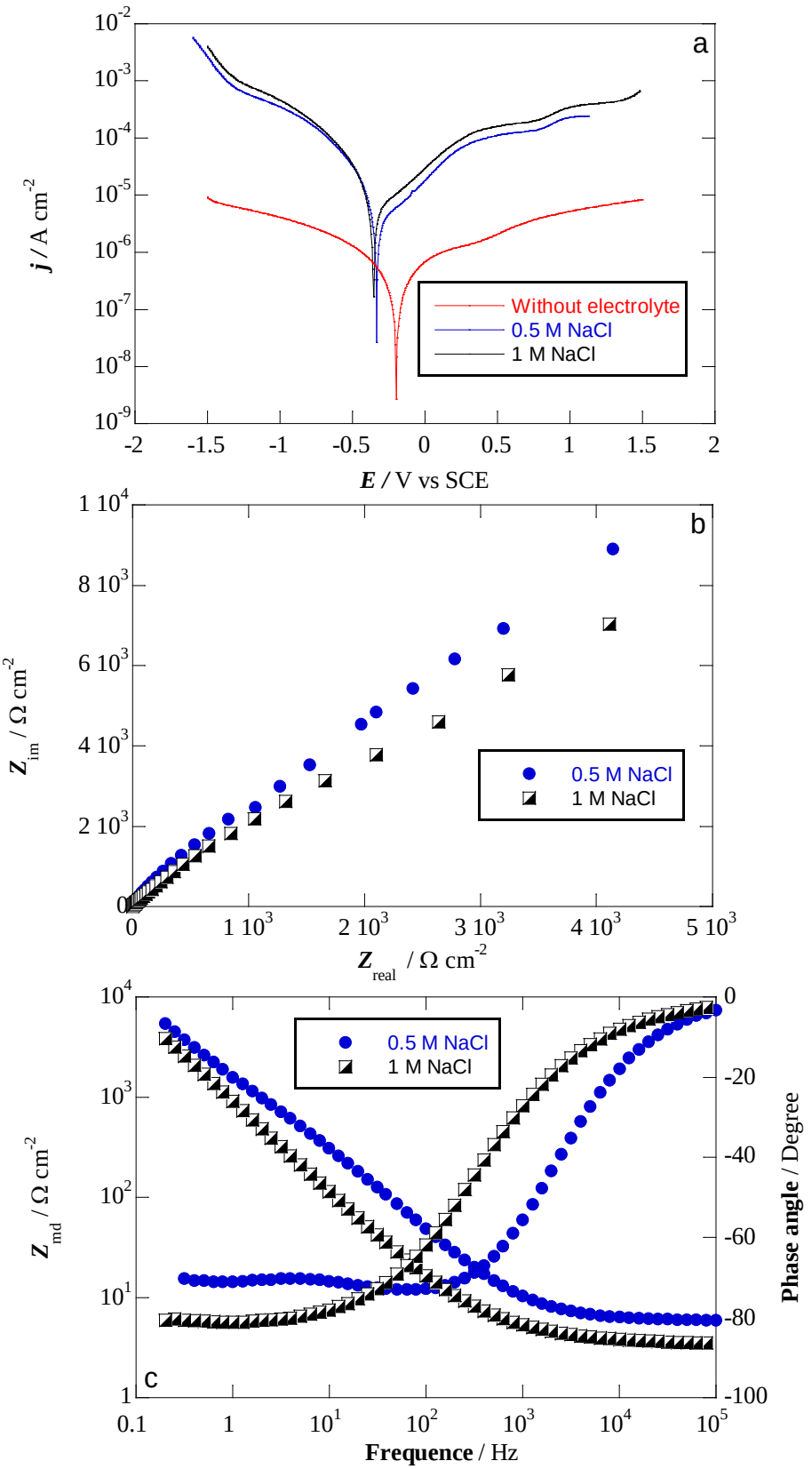
a
j / A cm-2
E / V vs SCE
Without electrolyte
0.5 M NaCl
1 M NaCl
b
Zim / Ω cm-2
Zreal / Ω cm-2
0.5 M NaCl
1 M NaCl
c
Zmd / Ω cm-2
Phase angle / Degree
Frequence / Hz
0.5 M NaCl
1 M NaCl

Fig. 2

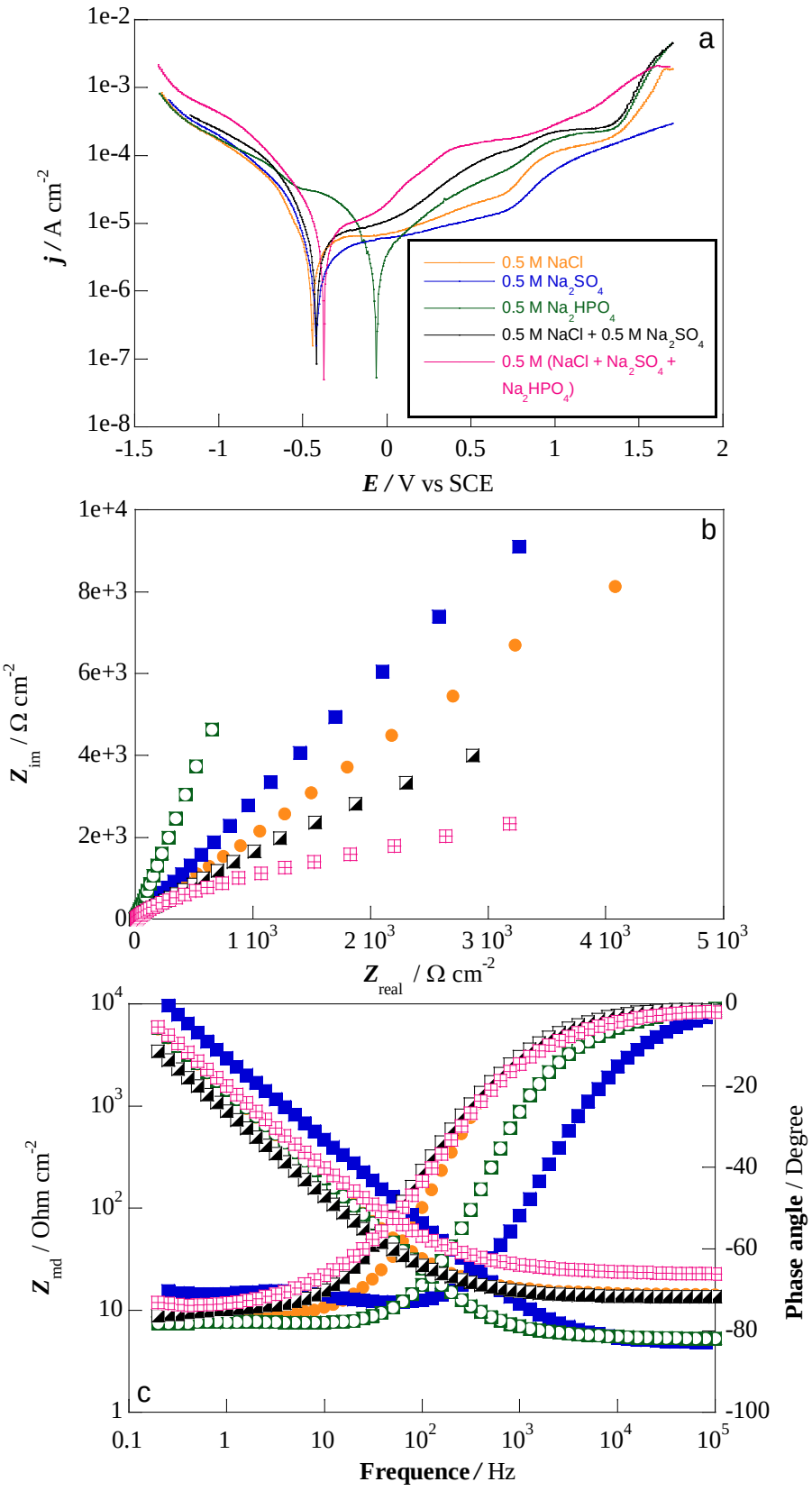
a
1e-2
1e-3
1e-4
1e-5
1e-6
1e-7
1e-8
j / A cm-2
-1.5
-1
-0.5
0
0.5
1
1.5
2
E / V vs SCE
0.5 M NaCl
0.5 M Na2SO4
0.5 M Na2HPO4
0.5 M NaCl + 0.5 M Na2SO4
0.5 M (NaCl + Na2SO4 + Na2HPO4)
b
1e+4
8e+3
6e+3
4e+3
2e+3
0
Z im / Ω cm-2
1 10^3
2 10^3
3 10^3
4 10^3
5 10^3
Z real / Ω cm-2
c
10^4
10^3
10^2
10
1
Z md / Ohm cm-2
0
-20
-40
-60
-80
-100
Phase angle / Degree
0.1
1
10
10^2
10^3
10^4
10^5
Frequence / Hz

Fig. 3

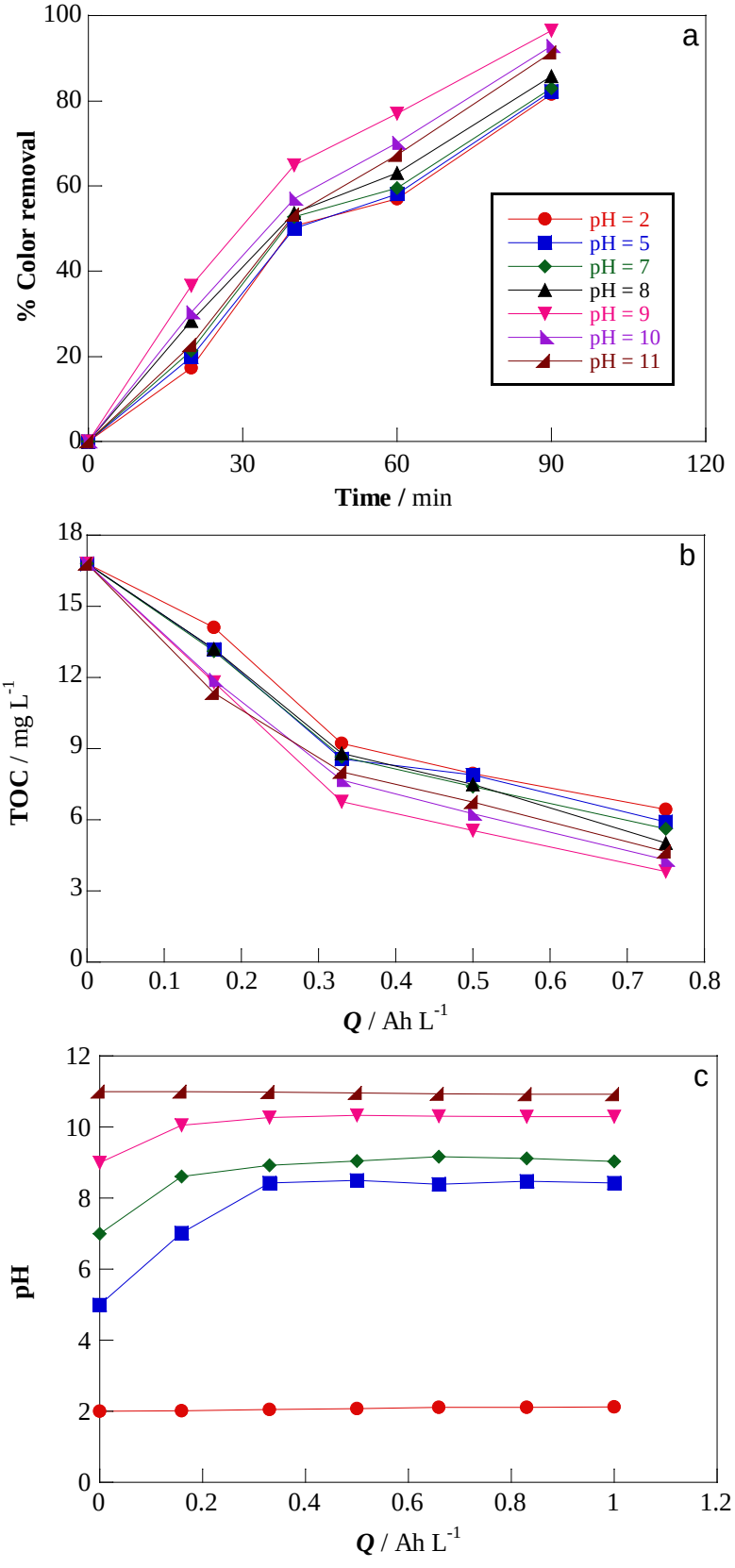
a
% Color removal
Time / min
pH = 2
pH = 5
pH = 7
pH = 8
pH = 9
pH = 10
pH = 11
b
TOC / mg L-1
Q / Ah L-1
c
pH
Q / Ah L-1

Fig. 4

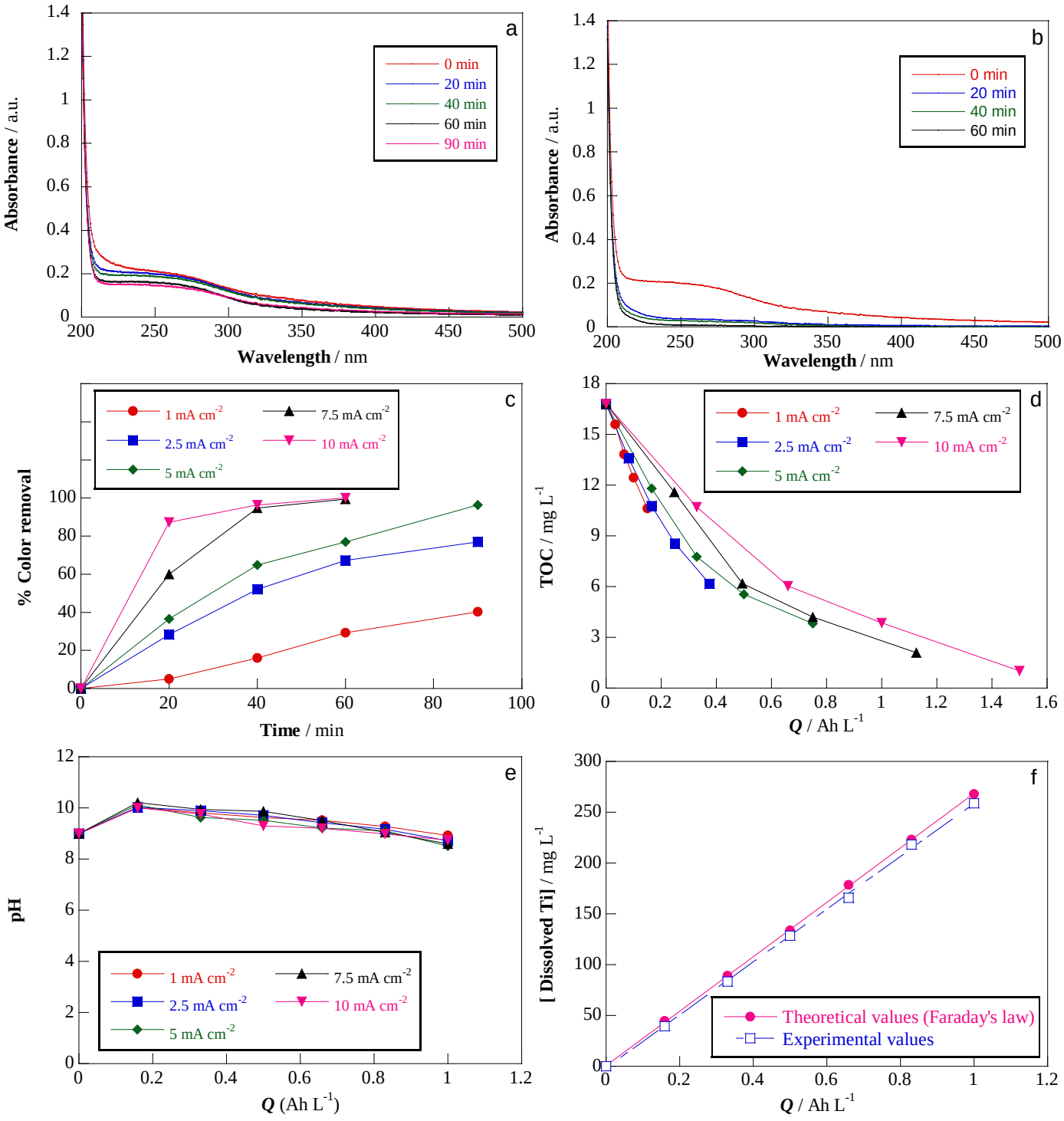
a
Absorbance / a.u.
Wavelength / nm
0 min
20 min
40 min
60 min
90 min
b
Absorbance / a.u.
Wavelength / nm
0 min
20 min
40 min
60 min
c
% Color removal
Time / min
1 mA cm-2
2.5 mA cm-2
5 mA cm-2
7.5 mA cm-2
10 mA cm-2
d
TOC / mg L-1
Q / Ah L-1
1 mA cm-2
2.5 mA cm-2
5 mA cm-2
7.5 mA cm-2
10 mA cm-2
e
pH
Q (Ah L-1)
1 mA cm-2
2.5 mA cm-2
5 mA cm-2
7.5 mA cm-2
10 mA cm-2
f
[Dissolved Ti] / mg L-1
Q / Ah L-1
Theoretical values (Faraday's law)
Experimental values

Fig. 5

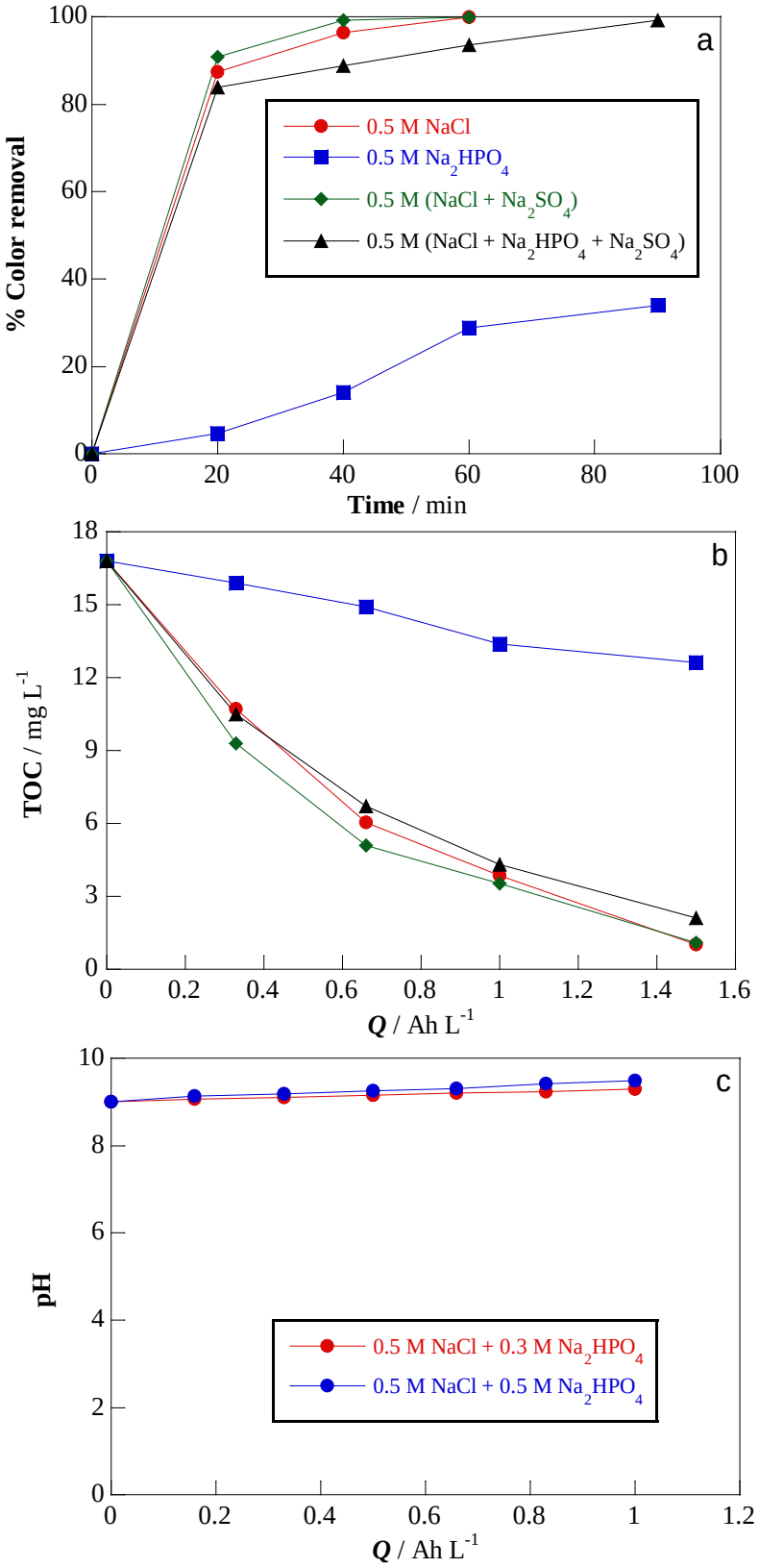
a
% Color removal
Time / min
0.5 M NaCl
0.5 M Na2HPO4
0.5 M (NaCl + Na2SO4)
0.5 M (NaCl + Na2HPO4 + Na2SO4)
b
TOC / mg L-1
Q / Ah L-1
c
pH
Q / Ah L-1
0.5 M NaCl + 0.3 M Na2HPO4
0.5 M NaCl + 0.5 M Na2HPO4

Fig. 6

673 **Table 1**

674 Results of potentiodynamic polarization for pure titanium as working electrode determined by the
675 Tafel extrapolation method in the presence of different supporting electrolytes (each at a
676 concentration of 0.5 M) at pH 9.0. Scan rate: 5 mV s^{-1}.

Electrolyte	E_{corr} (mV)	I_{corr} (μA cm^{-2})
Na_2SO_4	-325	0.106
NaCl	-398	0.149
Na_2HPO_4	-44	0.091
NaCl + Na_2SO_4	-405	0.152
NaCl + Na_2SO_4 + Na_2HPO_4	-386	0.146

677